Available online at www.sciencedirect.com

ScienceDirect

Procedia Engineering 173 (2017) 1266 – 1274

Procedia Engineering

www.elsevier.com/locate/procedia

11th International Symposium on Plasticity and Impact Mechanics, Implast 2016

Interface Mechanics and its Correlation with Plasticity in Polycrystalline Metals, Polymer Composites, and Natural Materials

Devendra Verma[a], Chandra Prakash[a], and Vikas Tomar[a*]

[a]School of Aeronautics and Astronautics, Purdue University, West Lafayette, IN 47907, USA;

Abstract

The interfaces in a composite material have finite thickness up to few micrometers, and have a significant effect on its mechanical strength. In this work, interfaces in polymer composites, and natural materials are analyzed under quasistatic and dynamic loading conditions to obtain interfacial constitutive response at strain rates from 10^{-2} to 10^{3} s^{-1} using a new technology called nanomechanical Raman spectroscopy. The interface stresses, interface elastic constants, and interface stress-strain is obtained for the glass/epoxy interfaces along with a power law constitutive model to predict the interface deformation behavior with a dependence on both strain rate and interface thickness.

Keywords: Raman spectroscopy, Interface mechanics, Interface stresses, High strain rate, Dynamic loading

* Corresponding author. Tel.: 1 765 494 3423
E-mail address: tomar@purdue.edu

Peer-review under responsibility of the organizing committee of Implast 2016

1. Introduction

Interfaces in the materials are known entities since last century described as early as in the interfacial excess energy formulations by Gibbs [1]. The interface effect (or surface effect) is also widely referred to as the interface stress (or surface stress) that consists of two parts, both arise from the distorted atomic structure near the interface (or surface): the first part is the interface (or surface) residual stress which is independent of the deformation of solids, and the second part is the interface (or surface) elasticity which contributes to the stress field related to the deformation. Plastic deformation, in particular, the initial yielding point (i.e. the yield surface), is sensitive to the local stress (or local strain) of a heterogeneous material, which includes both the local (surface/interface) residual stress and local stress–strain relationship. The plastic deformation at the interfaces also considers the tension and compression along the interface

Peer-review under responsibility of the organizing committee of Implast 2016
doi:10.1016/j.proeng.2016.12.152

and stress mismatch because of the material property differences. In the nanomaterials, the surface and interface stresses become even more important owing to the nanoscale size of the particles and interface areas.

The naturally occurring materials have been of keen interest in the materials community with the aim of understanding and reproducing the exceptional strength and toughening mechanisms present in exoskeletons of shrimps [2, 3], lobsters[4, 5], crabs[6, 7], nacre[8] etc. All these materials share some common traits such as a strong hierarchical structure, layered structure, composition of material with both minerals and fibers, gradient in the thickness of layers, etc. These naturally occurring materials have been able to manipulate the characteristics mentioned above to customize the design of their exoskeletons. The one important parameter along with the material composition in these design is the role of the interfaces in the multilayered structure. In our articles, we highlighted the difference between the mechanical properties of two similar species of shrimp Pandalus Platyceros and Rimicaris Exoculata, with interlayer structure as shown in Fig. 1 that are found at sea level and at 2300 m depth in the sea as a function of habitat, wet vs dry[2], and as a function of temperature[3], and as a function of mineral composition[9, 10]. The interfaces with different thickness and different phases were compared to study the effectiveness of the stress transfer of the layers as shown in.Fig. 1(b) A comprehensive study on these is given in the articles by Tao et al [11, 12].

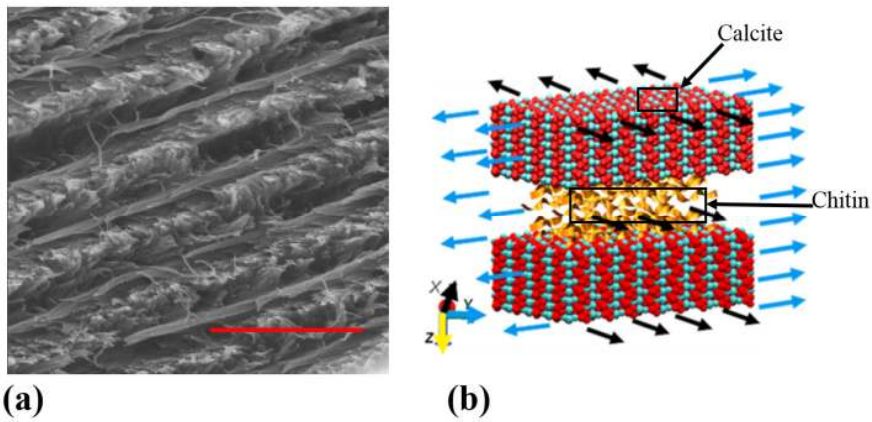

Fig. 1. (a) Interfacial structure in shrimp exoskeleton, and (b) interfacial molecular structure made of Calcite and Chitin.

In this article, a discussion is given on the interface mechanics. Nanomechanical Raman spectroscopy used in this paper to measure the interface stresses. A comparison between the numerically and experimentally measured interface elastic constants is presented in addition to the stress-stress response of interface and its effect on material properties of the interface and its adjacent phases.

2. Interface Stresses

Interfaces in composite materials can be considered as a material phase confined between two separate grains or phases. Single interface samples of glass and epoxy were prepared with an epoxy interface sandwiched between two glass phases. The samples were prepared using two-part industrial epoxy procured from Composite Polymer Design (South St. Paul, MN, USA). The resin, CPD4505A, and hardener, CPD 4507B, were thoroughly mixed in recommended proportions of 100A : 28B by weight. The epoxy layer thickness was controlled by putting tabs of appropriate thickness in between the glass slides. The samples were cured at a prescribed temperature of 250 ^{o}F for one day. The thickness of the interface in samples was measured with a microscope to make sure that it was in the error margin of 10±0.5 μm. The sample surfaces as shown in Fig. 2(a) were polished to remove scratches that could

interfere with the data measurement during experiments.

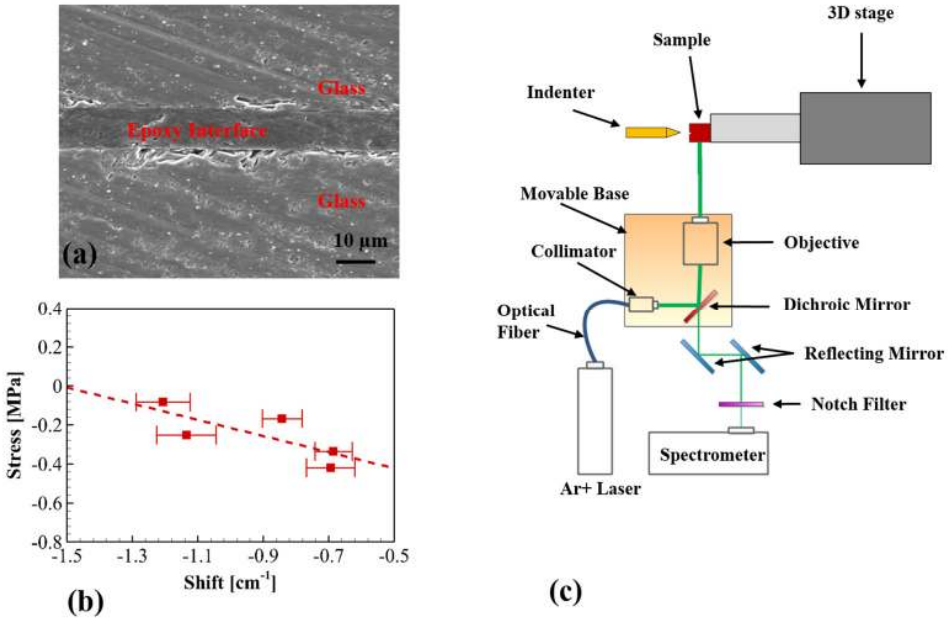

Fig. 2. (a) Image of the epoxy interface sample, (b) Raman shift-stress calibration curve, and (c) schematic of Raman measurements set up.

The Raman spectroscopy is based on 'Raman Effect', which provides a unique 'fingerprint' of every individual substance as a characteristic of for its identification.

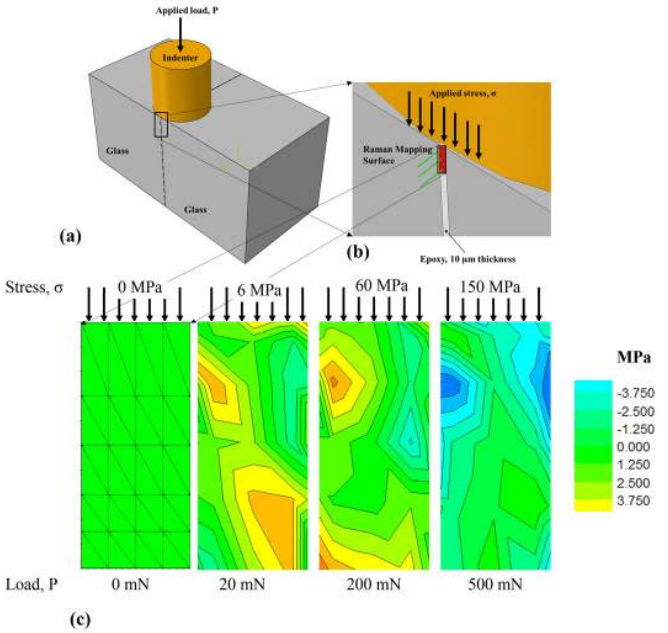

Fig. 3. Schematic of epoxy interface between glasses with the indenter direction, (b)the magnified region showing the area for Raman map collection and, (c) Raman stress map on the interface with applied load of 0, 20, 200, and 500 mN. The height in each map is 80 µm and width is 25 µm. Figure with 0 mN load shows the Raman data collection points.

It is an inelastic process in which energy is exchanged between the incident photon and molecule. We have used the Raman spectroscopy to measure the stresses in the interface at different applied loads during indentation to compare the stress distribution. The Mechanical load was applied using the nanoindentation platform manufactured by Micro Materials Inc., UK with load range from 0.1 mN to 500 mN, with the accuracy of better than 0.1 mN. The experimental setup to measure the Raman signal is shown in Fig. 2(c).

The first step to measure the stress across the interface is to establish a calibration curve of Raman shift with the applied stress. A uniaxial load was applied on a block of epoxy and the Raman shift was measured at applied loads of 100, 200, 300, 400 and 500 mN. The stresses were obtained by dividing the load by the area of the calibration sample. The measured Raman peak data was converted into shift by the equation

$$\Delta\omega = \left(\frac{1}{\lambda_{laser}} - \frac{1}{\lambda_{measured}} \right) * 10 \wedge 7 \; cm^{-1}. \tag{1}$$

The change in shift was obtained by subtracting the shift at the applied load for the shift at zero load. The calibration curve for shift versus load for epoxy is given in

Fig. 2(b). The measurements were performed on the epoxy interface while holding the load constant. The stress distribution across interfaces is shown in

Fig. 3(c). The load direction is from the top of the picture. The figure shows the average values of stresses as measured on the interface. This technique has been used in the literature to measure stresses tensors in the crystalline materials such as Silicon [13] but for the case polymers such as epoxy the average stresses can be measured [14].

The Raman spectroscopy only provides the average stress at the interface but stress tensors in different directions are needed to fully understand the behavior of interfaces. Even in the experiments, it is difficult to measure the lateral stresses. An analytical solution is therefore developed to calculate the lateral stresses during indentation of interfaces. A schematic of the contact problem of interface is illustrated in

Fig. 3. The details on the analytical solution are given in authors previous articles.

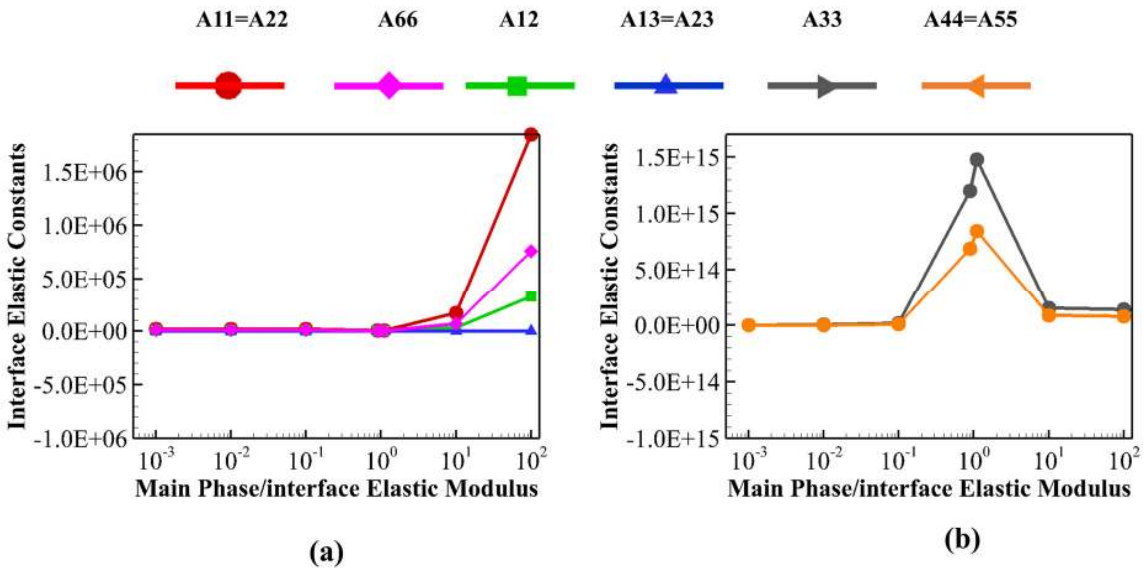

Fig. 4. Absolute values of Interface elastic constants calculated for different ratios of elastic modulus of main phase to interface with (a) plotting the elastic constants A11, A66, A12, A13, and (b) plotting A33 and A44.

3. Interface Elastic Constants

The interface elastic constants were calculated using equations in the article by Ustinov et al. [15] for different ratios of interface modulus as compared to the main phase. The results are given in Fig. 4 for the range of rations from 0.001 to 100. The absolute values of the interface elastic constants are also plotted to observe the variation with the change in the ratio as shown in Fig. 4. It can be seen that in the present isotropic material A11, A66, A12, A13 keeps decreasing as the modulus of both phases matches and then starts increasing again with the minimum at the point of same materials but the opposite is true for A33 and A44 with the maximum values at the point when the interface and bulk phase has the same properties.

The interface elastic constants by both Dingreville and Qu[16, 17] and K. B. Ustinov et al. [15] are calculated based on the strain energy. Per Dingreville, the interface contribution to the thermodynamic properties is defined as the excess over the values that would obtain if the bulk phases retained their properties constant up to an imaginary surface (of zero thickness) separating the two phases. The surface free (excess) energy of a near-surface atom is defined by the difference between its total energy and that of an atom deep in the interior of a large crystal. Surface free energy corresponds to the work of creating a unit area of surface, whereas surface stress is involved in computing the work in deforming a surface.

The interface elastic constants given in Table 1 are converted into surface constants based on equation from K. B. Ustinov et al. for a 10 micron thickness interface. The reduced modulus measured from the indentation experiments after conversion to surface constant is also listed in the same table for comparison. The interface constants after the conversion fall under the same order as the ones calculated from the analytical relations given for interfaces.

Table 1 *Comparison of interface elastic constants by both methods.*

	Analytical (This work)	**Theoretical Formula [15]**	**Theoretical Approximations [15]**	**Indentation Experiments (This work)**
A11 (Pa-m)	34029.1	-1253260.483	53571.42857	38195.94
A22 (Pa-m)	6821.673	-1253260.483	53571.42857	-
A33 (Pa/m)	2.03E+14	5.74205E+14	5.35714E+14	-
A13 (Pa)	2.8E+09	2208480565	3571428571	-

These results show the comparison between different formulations given in the literature and a first comparison with the experimental results. The interface stress contribution is well recognized but still there is more work needed to be able to address and implement the constitutive behavior of interfaces in the engineering problems. It has a very high potential of application in areas such as interface between glass/fiber in composites, interfaces at grain boundaries in metals to mention a few.

4. Interface Dynamic Properties

To understand the interface mechanical properties, an idealized system with epoxy interface between two glass slides was examined under static and dynamic loading. The sample surface is shown in Fig. 2(a). The impact experiments were performed on the epoxy interface to extract the stress-strain effect of the interface at different strain rates[18]. It was found that interfaces are affected by both strain rate and confinement effects during deformation. A new constitutive model is developed that couples the effect of both strain rate and lateral stresses given as

$$\sigma = (A + B\varepsilon^{n})(1 + C\ln\dot{\varepsilon}^{*})(1 + k\sigma_{1}^{*}). \tag{2}$$

Here, σ is the equivalent stress, ε is the equivalent plastic strain, A is the yield stress, B is the strain hardening constant, n is the strain hardening coefficient, C is the strain rate strengthening coefficient and k is the confinement factor. $\dot{\varepsilon}^* = \dfrac{\dot{\varepsilon}}{\dot{\varepsilon}_{ref}}$ is the dimensionless strain rate normalized with reference strain rate, $\sigma_1^* = \dfrac{\sigma_1}{\sigma_{compressive\,strength}}$ is the dimensionless lateral stress normalized with the compressive strength of the material. The reference strain rate is taken as 1 s^{-1} and $\sigma_{compressive\,strength}$ is taken as 100 MPa. In the current experiments, the temperature was constant so the temperature effects were neglected.

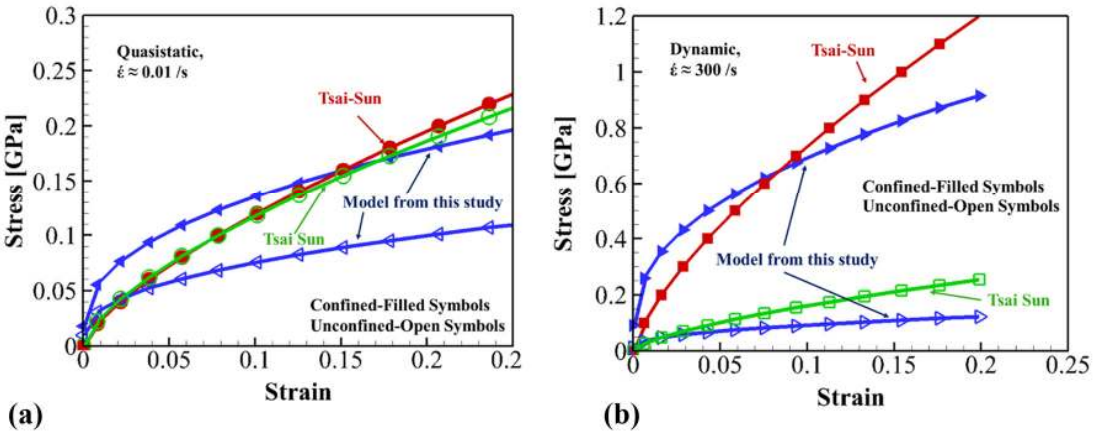

Fig. 5. Fit of the current model with stress strain for (a) quasistatic loading and (b) dynamic loading.

The stress strain response for the epoxy interface was analyzed at high and low strain rates as shown in Fig. 5 with the confined interface behavior labeled with closed symbols and unconfined epoxy behavior labeled with open symbols. At lower strain rates, the difference in stresses is mostly because of the confinement effect while in the dynamic case the strain rate effect also plays a major role. The difference in the stresses is higher in the dynamic case as evident in Fig. 5(b) compared to Fig. 5(a). It is also compared to the stress strain behavior fitted by Tsai-Sun model on the same plot. Thus, the current model is better suited to model the behavior of materials under confined spaces such as interfaces in the composite materials, metals, ceramics etc. A conventional way is to consider interface as a zero thickness and to not consider interface effect on the material deformation. The model in Eq. (2) takes into account the effect of interface mechanical properties on the mechanical deformation and should be considered for cases that have interface dominant geometries such as the biological materials analyzed in this work. The size effect of the interfaces is being analyzed by the authors and will be published in the future papers.

5. Conclusions

A new technique based on nanomechanical Raman spectroscopy is presented to calculate the interface stresses and elastic constants using an analytical model. The elastic constants are then compared with the strain energy frameworks provided in the literature. The comparison between both methods show the dependence of the interface elastic

constants on the thickness of the interface. The elastic constants calculated from the stress-strain data matches the theoretical values after the thickness effect correction.

The interfaces are believed to play an important role in the observed behavior. The role of interfaces is identified by performing experiments on an idealized system of glass-epoxy interfaces. The confinement effect on the interfaces along with the effect of strain-rate was found to play a major role in the deformation of the examined interfaces. A new model capturing both strain rate and confinement effects is developed for strain rates up to $10^3 s^{-1}$ in this paper to account for confinement effect and strain rate effect coupling.

Acknowledgements

Authors would like to thank their colleagues Yang Zhang, Sudipta Biswas, Debapriya Mohanty, Hao Wang and Bing Li for helpful discussions.

References

[1] Gibbs JW. The Collected Works of J. Willard Gibbs, Volume I: Thermodynamics, Yale University Press, 1928.
[2] Verma D, Tomar V. An investigation into environment dependent nanomechanical properties of shallow water shrimp (Pandalus platyceros) exoskeleton. Materials science & engineering C, Materials for biological applications, 2014, **44,** 371-9.
[3] Verma D, Tomar V. Structural-Nanomechanical Property Correlation of Shallow Water Shrimp (Pandalus platyceros) Exoskeleton at Elevated Temperature. Journal of Bionic Engineering, 2014, **11,** 360-70.
[4] Boßelmann F, Romano P, Fabritius H, Raabe D, Epple M. The composition of the exoskeleton of two crustacea: The American lobster Homarus americanus and the edible crab Cancer pagurus. Thermochimica Acta, 2007, **463,** 65-8.
[5] Raabe D, Romano P, Sachs C, Fabritius H, Al-Sawalmih A, Yi S-B, et al. Microstructure and crystallographic texture of the chitin–protein network in the biological composite material of the exoskeleton of the lobster< i> Homarus americanus</i>. Mater Sci Eng, A, 2006, **421,** 143-53.
[6] Mayer G. New toughening concepts for ceramic composites from rigid natural materials. Journal of the Mechanical Behavior of Biomedical Materials, 2011, **4,** 670-81.
[7] Chen P-Y, Lin AY-M, McKittrick J, Meyers MA. Structure and mechanical properties of crab exoskeletons. Acta Biomaterialia, 2008, **4,** 587-96.
[8] Flores-Johnson E, Shen L, Guiamatsia I, Nguyen GD. Numerical investigation of the impact behaviour of bioinspired nacre-like aluminium composite plates. Composites Science and Technology, 2014, **96,** 13-22.
[9] Verma D, Tomar V. A comparison of nanoindentation creep deformation characteristics of hydrothermal vent shrimp (Rimicaris exoculata) and shallow water shrimp (Pandalus platyceros) exoskeletons. J Mater Res, 2015, **30,** 1110-20.
[10] Verma D, Tomar V. An investigation into mechanical strength of exoskeleton of hydrothermal vent shrimp (Rimicaris exoculata) and shallow water shrimp (Pandalus platyceros) at elevated temperatures. Materials science & engineering C, Materials for biological applications, 2015, **49,** 243-50.
[11] Qu T, Verma D, Shahidi M, Pichler B, Hellmich C, Tomar V. Mechanics of organic-inorganic biointerfaces-Implications for strength and creep properties. Mrs Bulletin, 2015, **40,** 349-58.
[12] Qu T, Verma D, Alucozai M, Tomar V. Influence of interfacial interactions on deformation mechanism and interface viscosity in alpha-chitin-calcite interfaces. Acta Biomater, 2015, **25,** 325-38.
[13] Gan M, Tomar V. An in situ platform for the investigation of Raman shift in micro-scale silicon structures as a function of mechanical stress and temperature increase. Review of Scientific Instruments, 2014, **85,** 013902.
[14] Colomban P, Gouadec G, Mathez J, Tschiember J, Pérès P. Raman stress measurement in opaque industrial Cf/epoxy composites submitted to tensile strain. Composites Part A: Applied Science and Manufacturing, 2006, **37,** 646-51.
[15] Ustinov KB, Goldstein RV, Gorodtsov VA. On the Modeling of Surface and Interface Elastic Effects in Case of Eigenstrains. In: Altenbach H, Morozov FN, editors. Surface Effects in Solid Mechanics: Models, Simulations and Applications. Berlin, Heidelberg: Springer Berlin Heidelberg; 2013. p. 167-80.
[16] Dingreville R, Hallil A, Berbenni S. From coherent to incoherent mismatched interfaces: A generalized

continuum formulation of surface stresses. J Mech Phys Solids, 2014, **72,** 40-60.
[17] Dingreville R, Qu J. Interfacial excess energy, excess stress and excess strain in elastic solids: Planar interfaces. J Mech Phys Solids, 2008, **56,** 1944-54.
[18] Verma D, Singh J, Varma AH, Tomar V. Evaluation of Incoherent Interface Strength of Solid-State-Bonded Ti64/Stainless Steel Under Dynamic Impact Loading. Jom, 2015, **67,** 1694-703.